AIChE

Fe_2O_3 on Ce-, Ca-, or Mg-Stabilized ZrO_2 as Oxygen Carrier for Chemical-Looping Combustion Using NiO as Additive

Magnus Rydén
Dept. of Energy and Environment, Chalmers University of Technology, SE-412 96 Göteborg, Sweden

Erik Cleverstam and Marcus Johansson
Dept. of Chemical and Biological Engineering, Chalmers University of Technology, SE-412 96 Göteborg, Sweden

Anders Lyngfelt and Tobias Mattisson
Dept. of Energy and Environment, Chalmers University of Technology, SE-412 96 Göteborg, Sweden

DOI 10.1002/aic.12143
Published online January 8, 2010 in Wiley InterScience (www.interscience.wiley.com).

Oxygen-carrier particles for chemical-looping combustion have been manufactured by freeze granulation. The particles consisted of 60 wt % Fe_2O_3 as active phase and 40 wt % stabilized ZrO_2 as support material. Ce, Ca, or Mg was used to stabilize the ZrO_2. The hardness and porosity of the particles were altered by varying the sintering temperature. The oxygen carriers were examined by redox experiments in a batch fluidized-bed reactor at 800–950°C, using CH_4 as fuel. The experiments showed good reactivity between the particles and CH_4. NiO was used as an additive and was found to reduce the fraction of unconverted CH_4 with up to 80%. The combustion efficiency was 95.9% at best and was achieved using 57 kg oxygen carrier per MW fuel. Most produced oxygen carriers appear to have been decently stable, but using Ca as stabilizer resulting in uneven results. Further, particles sintered at high temperatures had a tendency to defluidize. © 2010 American Institute of Chemical Engineers *AIChE J,* 56: 2211–2220, 2010

Keywords: chemical-looping combustion, iron oxide, nickel oxide, zirconia, natural gas

Introduction

In recent years, concerns that emissions of CO_2 from combustion of fossil fuels may lead to changes in the climate of the earth have been growing steadily. As a consequence, a majority of the scientific community now conclude that global CO_2 emissions would need to be reduced greatly in the future.

One way to reduce CO_2 emissions that are receiving considerable interest is carbon capture and storage, which involves capturing of CO_2 in emission sources and storing it where it is prevented from reaching the atmosphere. For example, CO_2 could be captured in fuel gases from combustion or industrial processes and stored in geological formations, such as depleted oil fields or deep saline aquifers.

Chemical-looping combustion (CLC) involves oxidation of a fuel using oxygen from a solid oxygen carrier. In this way, the products are not diluted with N_2, and pure CO_2 for sequestration is obtained without the need for costly gas separation. Because of this favorable characteristic, CLC could

Correspondence concerning this article should be addressed to M. Rydén at magnus.ryden@chalmers.se.

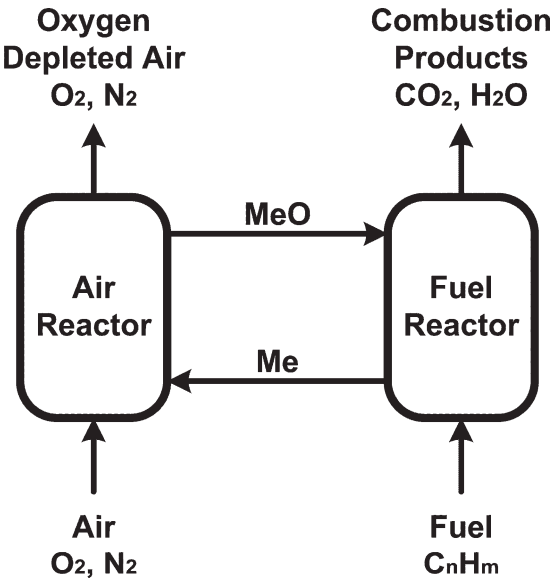

Figure 1. Schematic description of chemical-looping combustion.

have an important role to play in the global task to reduce anthropogenic CO_2 emissions.

Technical Background

Chemical-looping combustion

In CLC, two separate reactor vessels are used, one for air and one for fuel. A solid oxygen carrier performs the task of transporting oxygen between the reactors. Direct contact between fuel and air is avoided, so that the combustion products are not diluted with N_2, see Figure 1.

Typically, the abbreviation MeO is used to describe the oxygen carrier in its oxidized form, whereas Me is used for the reduced form. This is because many potential oxygen-carrier materials are metal oxides.

The oxygen carrier circulates between the reactors. In the fuel reactor, it is reduced by the fuel, which in turn is oxidized to CO_2 and H_2O according to reaction (1). In the air reactor, it is oxidized to its initial state with O_2 from the combustion air according to reaction (2).

$$C_nH_m + (2n + 1/2m)MeO \rightarrow nCO_2 + 1/2mH_2O + (2n + 1/2m)Me \quad (1)$$

$$Me + 1/2O_2 \rightarrow MeO. \quad (2)$$

The amount of energy released or required in each reactor vessel depends on the nature of the oxygen carrier and the fuel. Reaction (2) is always strongly exothermic. For most oxygen-carrier materials, reaction (1) is endothermic if the fuel is a hydrocarbon. Therefore, the flow of solid oxygen carrier is also needed to transfer sensible heat from the air reactor to the fuel reactor. The net energy released in the reactor system is the same as in ordinary combustion. This is apparent because combining reactions (1) and (2) yield reaction (3), which is complete combustion of the fuel with O_2.

$$C_nH_m + (n + 1/4m)O_2 \rightarrow nCO_2 + 1/2mH_2O. \quad (3)$$

Compared with conventional combustion, CLC has several potential benefits. The exhaust gas from the air reactor is harmless, consisting mainly of N_2 and possibly some O_2. There should be no thermal formation of NO_X because regeneration of the oxygen carrier takes place without flame and at moderate temperatures. The gas from the fuel reactor consists of CO_2 and H_2O, so cooling in a condenser is all that is needed to obtain almost pure CO_2.

CLC could replace ordinary combustion in many common large-scale applications. The main advantage would be more or less complete CO_2 capture, without necessarily decreasing the overall process efficiency. This is a rare feature among technologies proposed for CO_2 capture, which typically comes with considerable costs and energy penalties for gas separation. Because of this, CLC should be a very attractive technology for power generation with CO_2 capture of fossil fuels such as coal and natural gas. It could also be used for other large-scale applications, for example, combustion of waste products such as refinery gas, or for generation of heat to industrial processes or district heating systems. Another interesting option could be to use CLC as heat source for production of H_2 via the endothermic steam reforming reaction. This way it would be possible to produce H_2 from fossil fuels such as natural gas without CO_2 emissions to the atmosphere, which could be used as emission-free fuel for vehicles and other applications.

In practice, a CLC process could be designed in different ways, but circulating fluidized beds with oxygen-carrier particles used as bed material are likely to have an advantage over other alternatives as this design is well established, straightforward, provides good contact between gas and solids, and allows a smooth flow of oxygen-carrier particles between the air reactor and the fuel reactor.

Oxygen-carrier materials

A feasible oxygen-carrier material for CLC should have high reactivity with fuel and oxygen, be thermodynamically capable to convert a large share of the fuel to CO_2 and H_2O, have a sufficiently high mass fraction of oxygen, which can react according to reaction (1), have low tendency for fragmentation, attrition, agglomeration, and other kinds of mechanical or thermal degeneration, not promote extensive formation of solid carbon in the fuel reactor, and preferably be cheap and environmentally sound. Metal oxides, such as NiO, Fe_2O_3, Mn_3O_4, and CuO, supported on inert carrier material, such as Al_2O_3 or stabilized ZrO_2, are likely candidates to meet those criteria. An overview of the research treating these kinds of oxygen carriers can be found in the works of Cho,[1] Johansson,[2] and Adánez et al.[3] Information about additional potential oxygen-carrier materials can be found in the work of Jerndal et al.,[4] which includes a theoretical examination of 27 different oxide systems. Continuous CLC in circulating fluidized beds has been demonstrated by Lyngfelt et al.,[5] Ryu et al.,[6] Johansson et al.,[7,8] Abad et al.,[9,10] Adánez et al.,[11] Linderholm et al.[12,13] (Linderholm et al., Submitted), de Diego et al.,[14] Berguerand and Lyngfelt,[15,16] Rydén et al.,[17] Kolbitsch et al.,[18] and Pröll et al.[19]

Table 1. Summary of Oxygen Carrier Materials

Oxygen Carrier	Active Phase	Support Material	Sintering Temperature (°C)	Density (g/cm^3)	Porosity	Crushing Strength (N)
F6MZ1100	Fe_2O_3	Mg-ZrO_2	1100	2310	0.58	1.1
F6MZ1300	Fe_2O_3	Mg-ZrO_2	1300	3960	0.27	3.0
F6MZ1400	Fe_2O_3	Mg-ZrO_2	1400	4160	0.24	3.6
F6CeZ950	Fe_2O_3	Ce-ZrO_2	950	1840	0.66	0.6
F6CeZ1100	Fe_2O_3	Ce-ZrO_2	1100	2800	0.49	2.1
F6CaZ1100	Fe_2O_3	Ca-ZrO_2	1100	3050	0.54	2.4
N6AM1400	NiO	$MgAl_2O_4$	1400	3000	0.42	2.2

An overview of various subjects regarding CLC, such as design of experimental reactors, power production with CO_2 capture, use of solid fuels, chemical looping for production of H_2 and synthesis gas, and more about oxygen carriers, can be found in the Doctoral theses by Brandvoll,[20] Johansson,[21] Wolf,[22] Kronberger,[23] Naqvi,[24] Leion,[25] and Rydén.[26]

Mixed oxides as oxygen carrier

A mixed-oxide oxygen carrier for CLC consists of more than one active phase and should be able to take advantage of favorable characteristics of each, that is, create some kind of positive synergy effect. Mixed oxides could be produced in different ways, for example, by mixing different oxygen-carrier particles in a fluidized bed, by impregnating a second active phase onto existing particles, or by producing materials with multiple active phases directly in the manufacturing process.

There are many synergy effects that could possibly be achieved. Jin et al.[27] prepared a CoO-NiO particle on yttria-stabilized zirconia, which reportedly suppressed formation of solid carbon on the particle surface. Son and Kim[28] applied NiO and Fe_2O_3 in different ratios onto bentonite, using NiO to provide high reactivity and Fe_2O_3 to improve the particle strength. Adánez et al.[29] added CuO to a NiO-based oxygen carrier to improve the conversion of CO and H_2, which is thermodynamically constrained for NiO.

In the study presented here, another approach is used. When reduced by a fuel, NiO is converted directly to metallic Ni, which is well known to catalyze decomposition of CH_4 and other hydrocarbons. Mattisson et al.[30] found that almost complete conversion of CH_4 into combustion products can be achieved with a very small bed of NiO material, and that the reaction proceeds with CO and H_2 as intermediates. Unfortunately, using NiO as oxygen carrier for CLC has some drawbacks. NiO is comparably expensive and also a health hazard. Further, the conversion of hydrocarbons into H_2O and CO_2 at relevant temperatures is limited to slightly above 99% because of thermodynamical constraints. In contrast, Fe_2O_3 is cheap, abundant, nontoxic, and can convert hydrocarbon fuel completely into CO_2 and H_2O. According to Mattission et al.,[31] the reactivity with CH_4 is low compared with NiO, but the reactivity with CO and H_2 has been found to be high. Therefore, it seems reasonable to believe that the rate-limiting step for CLC of hydrocarbons using Fe_2O_3 as oxygen carrier is conversion of CH_4 into reactive intermediates, such as CO and H_2, see Johansson et al.[32] Based on these characteristics, a mixed-oxide oxygen carrier that consists of small amounts of NiO as catalytic material and Fe_2O_3 as the main oxygen carrier could have advantages compared with the alternatives. Small amounts of NiO would likely be sufficient to facilitate decomposition of hydrocarbons and CH_4 into CO and H_2, which reacts fast with Fe_2O_3. In a study by Johansson et al.,[33] it was found that addition of as little as 1 wt % NiO to a sample of Fe_2O_3 improved the capacity of the sample to convert CH_4 into CO_2 and H_2O considerably. If feasible, such a mixed-oxides oxygen-carrier system could lower the cost for and potential environmental impact of oxygen-carrier materials considerably.

The aim of this study

The objective of this study is to examine Fe_2O_3 supported on stabilized ZrO_2 as oxygen-carrier material for CLC and also to examine if it is possible to improve the reactivity between Fe_2O_3 and CH_4 by addition of small amounts of catalytic NiO.

Experimental

Oxygen-carrier materials

The oxygen-carrier particles were prepared by dispersing fine chemical powders in a water-based slurry. After milling and addition of a binding agent, spherical particles were produced from the slurry by freeze granulation. The resulting particles were sintered for 6 h to improve their mechanical strength. A summary of produced particles can be found in Table 1.

All oxygen carriers produced consisted of 60 wt % active phase and 40 wt % inert support material. Sintering temperatures between 950 and 1400°C was used and is indicated by the four last digits in the designation of each material. The density is approximated by weighing a certain volume of particles and dividing the result with a factor of 0.63, which corresponds to good packing of spherical particles. Porosity is estimated by dividing the calculated density of the particle with the density of the solid, that is, a low porosity number reflects a particle with low porosity and vice versa. Crushing strength was measured directly and reflects the average force that is needed to crush a particle in the size span 180–250 μm. For most experimental work, particles in the size span 125–180 μm were used.

When used as oxygen carrier, iron oxide can be reduced in several steps. For CLC, only the first step, reduction of Fe_2O_3 to Fe_3O_4, is of interest. Further reduction to FeO and metallic Fe should be avoided, because formation of FeO could result in fluidization problems and also in poor conversion of the fuel due to less favorable thermodynamics. By contrast, NiO is reduced directly to metallic Ni and cannot

Table 2. Summary of Batch Experiments

Sample	Additive	T (°C)	Size (μm)	Reductions
F6MZ1100		950	125–180	14
F6MZ1100		950	90–125	14
F6MZ1100		850–950	180–250	15
F6MZ1100	5 wt % N6AM1400	950	125–180	8
F6MZ1100	5 wt % N6AM1400	950	125–180	8
F6MZ1100	5 wt % N6AM1400	800–950	180–250	16
F6MZ1300		950	125–180	9
F6MZ1400		950	125–180	14
F6CeZ950		950	125–180	14
F6CeZ1100		950	125–180	14
F6CeZ1100	5 wt % N6AM1400	950	125–180	14
F6CaZ1100		950	125–180	14
F6CaZ1100	5 wt % N6AM1400	950	125–180	14

be reduced further. A summary of the expected reduction reactions can be found in Table 3 later.

Reactivity tests in batch fluidized-bed reactor

The experiments were conducted in an 820-mm long quartz reactor with an inner diameter of 22 mm. A porous quartz plate, on which the oxygen-carrier sample is applied, is located 370 mm above the bottom. During operation, the sample is fluidized by adding gas to the bottom of the reactor, and the porous plate acts as gas distributor. To reach suitable temperature, the reactor is placed inside an electrically heated furnace. Reactor temperature is measured below and above the porous plate, using thermocouples enclosed in quartz shells. The pressure drop over the bed is measured with pressure transducers. The gas from the reactor is led to a cooler, in which the water is removed. Following this step, the volumetric flow of gas is measured, and the composition analyzed. The concentrations of CO_2, CO, and CH_4 are measured using infrared analyzers, whereas O_2 is measured with paramagnetic sensors.

The aim of the batch experiment was to examine the oxidation and reduction behavior of the oxygen carrier and to examine if the reactivity could be improved by adding NiO. To do so, a sample of 15 g particles was applied to the porous plate. Then, the reactor was heated to the desired temperature, which for these experiments was 800–950°C. During this period, the reactor was fluidized with inert N_2. CLC was simulated by alternating between reducing and oxidizing conditions. First, the sample was reduced with 0.45 L_n/min CH_4 for 30–40 s. The amount of oxygen carrier corresponds to 57 kg per MW added fuel.

Table 3. Expected ω for Various Reactions and Oxygen Carriers

Reaction	ω_{F6x}	$\omega_{N6AM1400}$	$\omega_{95/5\ F6x/N6AM1400}$
$NiO \rightarrow Ni + 1/2\ O_2$	–	1.000–0.872	1.000–0.994
$3\ Fe_2O_3 \rightarrow 2\ Fe_3O_4 + 1/2\ O_2$	1.000–0.980	–	0.994–0.975
$Fe_3O_4 \rightarrow 3\ FeO + 1/2\ O_2$	0.980–0.940	–	0.975–0.937
$FeO \rightarrow Fe + 1/2\ O_2$	0.940–0.820	–	0.937–0.822

Following the reduction period, the sample was reoxidized with 1.0 L_n/min of a gas mix consisting of 5 vol % O_2 and 95 vol % N_2. The reason for not using air is that reaction (2) is highly exothermic, so a low concentration of O_2 is used to avoid extensive heating of the reactor. After the oxidation period, the sample was ready to be reduced again and so on. To avoid oxygen and methane mixing during the shifts between reduction and oxidation, 0.45 L_n/min N_2 was introduced during 180 s after each reduction and each oxidation period.

During reduction, the superficial gas velocity in the reactor was 0.082 m/s in the bottom of the reactor. As can be seen in Eq. 1, there is a volumetric increase as the fuel reacts with the oxygen carrier. If there is 100% conversion of the fuel, the superficial gas velocity in the top of the bed will be 0.247 m/s. During oxidation, the superficial gas velocity is 0.174–0.183 m/s, depending on how much O_2 that reacts with the oxygen carrier. The static bed height was 11–26 mm, depending of the density of the oxygen carrier. During operation, the bed is fluidized within the bubbling region and is expected to expand 10–20%. The minimum fluidization velocity of used oxygen carriers depends on factors such as particle diameter, particle density, and fluidization gas. For the particles used here, it was in the range of 0.005–0.025 m/s.

A summary of experiments conducted can be found in Table 2.

Evaluation of data

The oxygen ratio, R_0, is defined in Eq. 4, and the degree of oxidation of the oxygen carrier, X, is defined in Eq. 5.

$$R_0 = (m_{s,ox} - m_{s,red})/m_{s,ox} \tag{4}$$

$$X = \frac{m_s - m_{s,red}}{m_{s,ox} - m_{s,red}}. \tag{5}$$

In Eqs. 4 and 5, m_s is the actual mass of sample, $m_{s,ox}$ is the mass of the sample when fully oxidized, and $m_{s,red}$ is the mass of the sample while completely reduced. R_0 describes the mass fraction of the particle that can theoretically be released as oxygen during operation. X describes the oxygen content of a sample relative to the theoretical maximum R_0. X can be calculated as a function of time using Eq. 6.

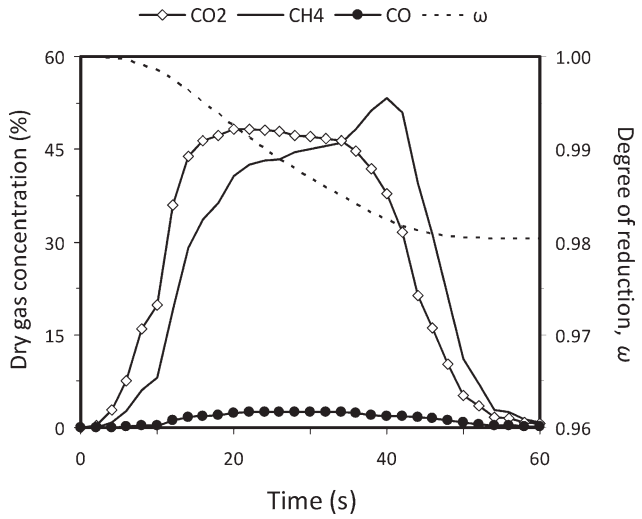

Figure 2. Reduction of 15 g F6MZ1100 with 0.45 L_n/min CH_4 at 950°C.

Data for third reduction cycle.

$$X_i = X_{i-1} - \int_{t_o}^{t_1} \frac{n_{\text{out,tot}}}{n_{\text{o,oc}} \times P_{\text{tot}}} \times (4p_{\text{CO}_2,\text{fr}} + 3p_{\text{CO,fr}} - p_{\text{H}_2,\text{fr}})dt. \tag{6}$$

In Eq. 6, X_i is the conversion as a function of time for period i, X_{i-1} is the conversion after the preceding period, t_0 and t_1 are the times for the start and finish of the period, respectively, $n_{\text{o,oc}}$ is the moles of active oxygen in the unreacted oxygen carrier, $n_{\text{out,tot}}$ is the molar flow of the gas leaving the reactor after the water has been removed, P_{tot} is the total pressure, and $p_{\text{CO}_2,\text{fr}}$, $p_{\text{CO,fr}}$, and $p_{\text{H}_2,\text{fr}}$ are the outlet partial pressures of CO_2, H_2, and CO after the removal of H_2O. $p_{\text{H2,fr}}$ was not measured online but assumed to be related to the outlet partial pressure of CO and CO_2 through an empirical relation based on the equilibrium of the gas-shift reaction.

In this article, the mass-based degree of reduction, ω, is used to describe the reduction of the oxygen-carrier particles. ω describes how much oxygen that has been removed from the oxygen carrier compared to its oxidized weight and is defined in Eq. 7.

$$\omega = \frac{m_{\text{s}}}{m_{\text{s,ox}}} = 1 + R_{\text{o}}(X - 1). \tag{7}$$

The mass conversion ω for various reduction steps can be found in Table 3, in which it has been assumed that the main oxygen carrier consists of Fe_2O_3, and that reduction of NiO to Ni is fast and takes place before reduction of Fe_2O_3 to Fe_3O_4.

In Table 3, F6x represents any kind of oxygen carrier that consists of 60 wt % Fe_2O_3, that is, the oxygen carriers examined in this study. It can be seen that ω below 0.980 should be avoided for experiments without addition of N6AM1400, while the corresponding number for experiments with addition of N6AM1400 is 0.975. Below these numbers, formation of FeO could be expected, which could result in defluidization of the sample and in poor conversion of the fuel due to less favorable thermodynamic conditions.

The CO_2 yield, γ_{red}, is defined in Eq. 8, and the CO share of carbon not converted into CO_2, ζ_{CO}, is defined in Eq. 9.

$$\gamma_{\text{red}} = p_{\text{CO}_2,\text{out}}/(p_{\text{CH}_4,\text{out}} + p_{\text{CO}_2,\text{out}} + p_{\text{CO,out}}) \tag{8}$$

$$\varsigma_{\text{CO}} = p_{\text{CO,out}}/(p_{\text{CH}_4,\text{out}} + p_{\text{CO,out}}). \tag{9}$$

A γ_{red} of 1 is desirable and corresponds to complete combustion of the fuel. A ζ_{CO} of 1 means that all carbon that is not converted into CO_2 is CO, whereas a ζ_{CO} of 0 means that it is CH_4.

The performance of a CLC process can also be expressed with the combustion efficiency, γ_{eff}, which is defined in Eq. 10.

$$\gamma_{\text{eff}} = 1 - \frac{n_{\text{CH}_4,\text{fr}} \times H_{\text{lhw,CH}_4} + n_{\text{CO,fr}} \times H_{\text{lhw,CO}} + n_{\text{H}_2,\text{fr}} \times H_{\text{lhw,H}_2}}{n_{\text{fuel,in}} \times H_{\text{lhw,fuel}}}. \tag{10}$$

The combustion efficiency basically describes the conversion of the fuel into reagents with the lower heating value as basis.

Results

Reduction experiments with CH_4

By themselves, the iron oxide particles showed decent reactivity with CH_4. Example of a typical reduction curve, in this case for F6MZ1100, can be found in Figure 2.

In Figure 2, it can be seen that it took a few seconds until high values of CO_2 and CH_4 were measured. This was due to imperfect plug flow and backmixing. The conversion into CO_2 was highest in the beginning of the reduction cycle and decreased as oxygen was removed from the oxygen carrier.

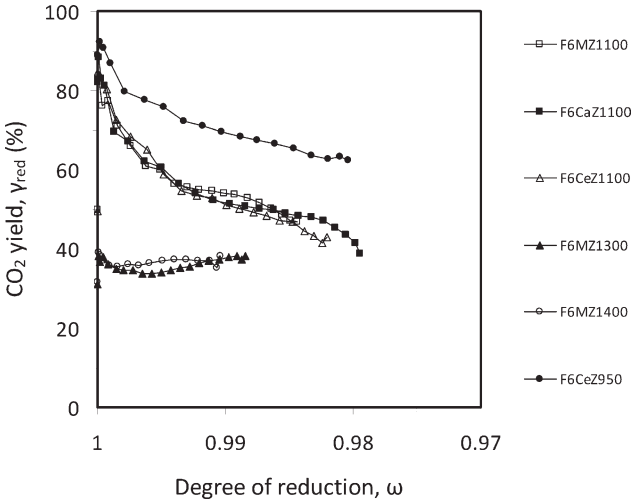

Figure 3. γ_{red} as a function of ω for examined oxygen carriers at 950°C.

Data for third reduction cycle.

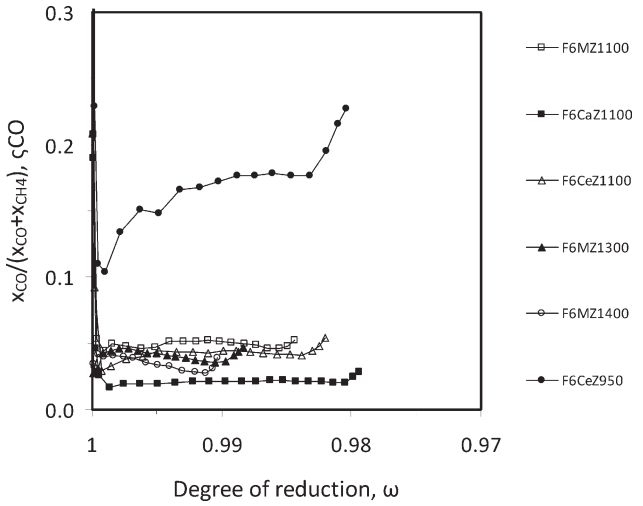

Figure 4. ζ_{CO} as a function of ω for examined oxygen carriers at 950°C.

Data for third reduction cycle.

The other oxygen-carrier particles examined sintered at 1100° provided very similar results, regardless of what doping material had been used to stabilize the ZrO_2. CO was low during the whole reduction period.

For particles sintered at different temperatures, there were some variations in the conversion level of CH_4 to CO_2. A summary for all examined oxygen carriers can be found in Figures 3 and 4, where γ_{red} and ζ_{CO} are shown as a function of ω, respectively.

In Figures 2 and 3, it can be seen that the conversion of CH_4 to CO_2 typically was highest in the beginning of the reduction cycle, when ω was close to 1, then decreased slowly as the particle was reduced. The effect was less apparent for particles sintered at high temperature though.

The first data points in Figures 3 and 4, those for which γ_{red} is above 80%, refer to the period when there was still N_2 present in the reactor due to back-mixing, that is, the period prior to $t = 15$ s in Figure 2. Once the system was free from N_2, γ_{red} typically was ≈75% for particles sintered at 1100°C.

In Figures 3 and 4, it can be seen that increasing the sintering temperature to 1300–1400°C decreased the reactivity of the oxygen carrier, whereas reducing the sintering temperature to 950°C increased it. This could be expected because high sintering temperature typically results in hard and comparably nonporous particles and thus reduce the active particle surface. Further, F6CeZ950 produced significantly more CO, compared with particles sintered at higher temperatures.

In Figure 5, γ_{red} as a function of ω for 14 reduction cycles for F6MZ1100 at different temperature levels is shown.

In Figure 5, it can be seen that reduced reactor temperature resulted in reduced rate of reaction, that is, the CO_2 yield is higher and the sample does not reach equally low ω. This could be expected, because chemical reaction in general proceeds faster at high temperatures. CO remained low during the whole reduction period at all temperatures.

Effect of N6AM1400 addition

Produced gas composition during reduction of F6MZ1100 with 5 wt % addition of NiO-based N6AM1400 particles at 950°C is shown in Figure 6.

γ_{red} as a function of ω for a few reduction cycles at various temperatures for the same particle is shown in Figure 7, whereas the corresponding ζ_{CO} as a function of ω is shown in Figure 8.

In Figures 6–8, it can be seen that CO_2 concentrations over 90 vol % were obtained for the mixture of F6MZ1100 and N6AM1400. Typically, y_{red} was ≈93% and y_{eff} was ≈95%. Further, unlike experiments without addition of N6AM1400 such as those shown in Figures 3 and 5, high conversion into CO_2 was sustained for a longer period of time and larger ω interval.

In Figure 7, it can be seen that the effect of reduced temperature was much less apparent compared with experiments without addition of N6AM1400, such as those presented in Figure 5. The difference in y_{red} between experiments conducted at 850 and 950°C was only a few percentage points.

In Figures 6 and 8, it can be seen that initially some CH_4 passed unreacted through the bed, but as N6AM1400 was reduced and metallic Ni was formed, eventually all CH_4 were decomposed into CO and H_2 instead, which could be expected.

For experiments with other oxygen carriers, the effect of adding N6AM1400 was less clear. For F6CeZ1100, addition of N6AM1400 did not have any immediate effect. However, after eight reductions, the CH_4 conversion increased somewhat, although to a much lesser extent than for F6MZ1100. For F6CaZ1100, addition of N6AM1400 did not have any effect during the initial eight reduction cycles. However, from the ninth cycle and on, there was a large improvement in the conversion of CH_4 and a large increase in the produced CO concentration. It is hard to draw any conclusions from these results though, because F6CaZ1100 experienced considerable physical changes during the course of the experiments, as will be explained later.

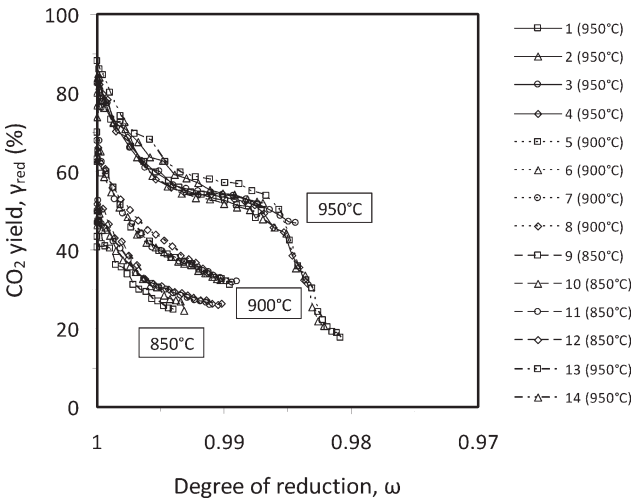

Figure 5. γ_{red} as a function of ω for F6MZ1100 for different reduction cycles and temperatures.

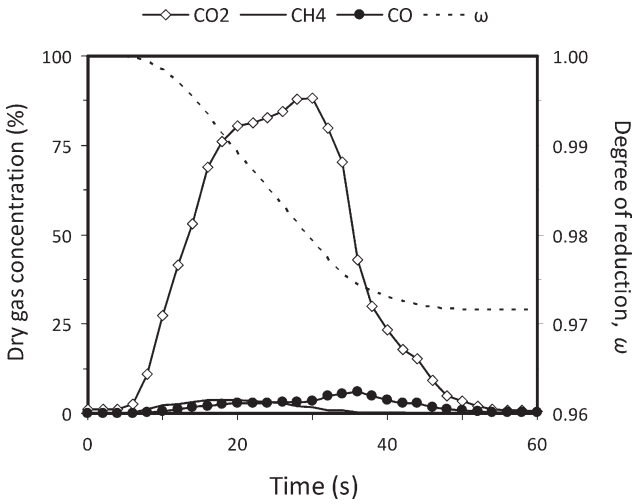

Figure 6. Reduction of 14.25 g F6MZ1100 and 0.75 g N6AM1400 with 0.45 L_n/min CH_4 at 950°C.

Data for third reduction cycle.

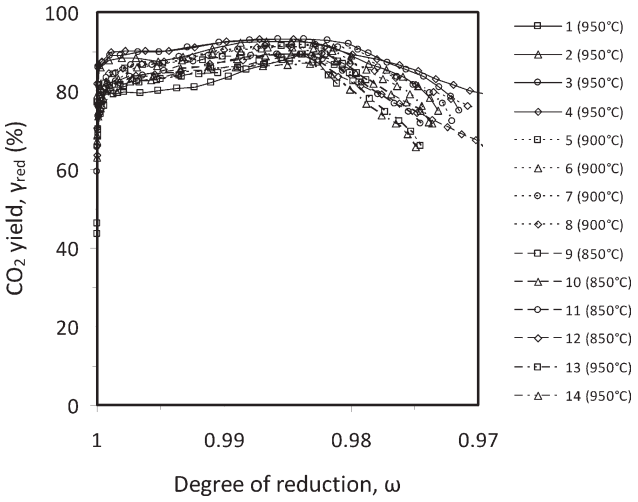

Figure 7. γ_{red} as a function of ω for 14.25 g F6MZ1100 and 0.75 g N6AM1400 for different reduction cycles and temperatures.

In Table 4, some performance data for F6MZ1100 derived from reductions such as those shown in Figures 2–8 are shown.

In Table 4, $\gamma_{eff,max}$ is the highest combustion efficiency measured during reduction of only F6MZ1100, following the period for which the products were still diluted with N_2, as explained earlier. $\gamma_{eff,max,mo}$ is the corresponding peak value for the case with 5 wt % N6AM1400 addition. $v_{CO_2,30s}$ and $v_{CO_2,30s,mo}$ are the volumes of CO_2 produced during 30 s of reduction expressed in normal liters.

The improvement in combustion efficiency, χ, describes the reduction in unconverted fuel passing through the reactor when the reactivity is at its highest and is defined in Eq. 11.

$$\chi = 100 \times (\gamma_{eff,max,mo} - \gamma_{eff,max})/(100 - \gamma_{eff,max}). \quad (11)$$

In Table 4, it can be seen that adding 5 wt % N6AM1400 had a positive effect on the fuel conversion when F6MZ1100 was used as oxygen carrier. The fraction of unconverted fuel was reduced with roughly 80%, as indicated by χ, which is a considerable improvement. However, it can be argued that this is insufficient proof that there is an actual synergy effect of mixing NiO and Fe_2O_3 as discussed in the introduction, that is, that metallic Ni converts CH_4 to CO and H_2, which subsequently reacts with Fe_2O_3. This is because Ni-based materials have higher reactivity and oxygen transfer capacity than the Fe_2O_3-based materials. Therefore, it could be expected that the addition of such a material should result in increased fuel conversion, even if there is no synergy effect.

One way of demonstrating that there is really a synergy effect is to show that there is an improvement in reactivity, even after subtracting the possible direct contribution of added NiO. This was done by calculating the increase in CO_2 production over a certain reduction period, σ, and is defined in Eq. 12.

$$\sigma = 100 \times [(v_{CO_2,30s,mo} - v_{CO_2,NiO})/v_{CO_2,30s} - 1]. \quad (12)$$

σ describes the increase in the total amount of CO_2 produced during 30 s, which is achieved by addition of 5 wt % N6AM1400. In Eq. 12, $v_{CO_2,\ NiO}$ reflects the contribution of oxygen-carrier capacity brought by the NiO addition, if it is assumed that added NiO is reduced to Ni by the fuel and that the products of this process are only CO_2 and H_2O. When the fuel is CH_4, $v_{CO_2,NiO}$ is 0.0342 L_n for 0.75 g N6AM1400.

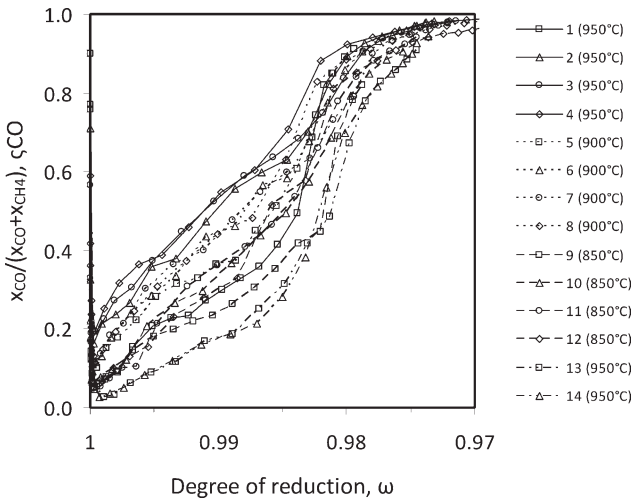

Figure 8. ζ_{CO} as a function of ω for 14.25 g F6MZ1100 and 0.75 g N6AM1400 for different reduction cycles and temperatures.

Table 4. Performance Data for F6MZ1100

	T_{fr} (°C)	$\gamma_{eff,max}$ (%)	$\gamma_{eff,max,\ mo}$ (%)	$v_{CO_2,30s}$ (L_n)	$v_{CO_2,30s,mo}$ (L_n)	χ (%)	σ (%)
F6MZ1100	950	75.3	95.9	0.096	0.128	83	−2
F6MZ1100	850	56.0	91.3	0.036	0.147	80	213

Data for third reduction.

In Table 4, it can be seen that there was no provable synergy effects at 950°C, but that σ was more than 200% for F6MZ1100 at 850°C. This means that more than three times as much CO_2 was produced for an experiment with N6AM1400 addition compared to one without, even with the additional oxygen-carrier capacity provided with NiO addition taken into consideration. Therefore, it seems safe to conclude that mixing NiO and Fe_2O_3 really did create a positive synergy effect. The absence of a verifiable synergy effect at 950°C was likely a result of the chosen experimental conditions. At 950°C, F6MZ1100 already provided decently high fuel conversion, even without addition of NiO. Therefore, the possible improvements were in the same order of magnitude as the extra oxygen-carrier capacity provided by the NiO particles, and the apparent synergy effect became zero.

Effect of particle size

As can be seen in Table 2 earlier, F6MZ1100 of three different size intervals were examined. All worked fine, and no significant differences could be verified between the different cases.

Oxidation of reduced particles

Reoxidation of reduced particles was an undramatic process. Basically, the oxidation reaction was sufficiency fast for all added O_2 to react with the particles, until they were completely reoxidized. No CO_2 or CO was formed during reoxidation, so there was no carbon deposition during the reduction period.

Fluidization properties and particle stability

During the course of the experiments, F6MZ1100, F6CeZ1100, and F6CeZ950 fluidized well and provided reasonably stable results, that is, each reduction and oxidation looked pretty much the same. For F6MZ1100, there was a slight increase in the CO concentration for each reduction, but it was marginal. Used particles of these three materials had 10–20% lower density compared with fresh ones, so obviously the pore structure of the particles was affected by the thermal or chemical conditions. Such changes are often seen during the initial reduction and oxidation cycles for experiments of this kind. It seems reasonable to believe that the particles would have stabilized themselves after a certain number or reductions and oxidations.

F6MZ1300 and F6MZ1400 experienced fluidization problems. After eight reductions, both these particles defluidized, and the fluidization could not be restarted. Further, F6MZ1400 also occasionally defluidized in the inert phase. One possible reason for this behavior could be that these two particles had considerably higher density compared with the other, as can be seen in Table 1. Therefore, they should require somewhat higher gas flows to fluidize properly. The superficial gas velocity was still at least two to three times higher than the theoretical minimum fluidization velocity though.

F6CaZ1100 initially worked well, but after eight reductions the CO concentration increased dramatically. It is possible that the particles became reduced too far, forming FeO, which could have resulted in various problems. For the experiment with addition of N6AM1400, obtained results were also confusing with a radical change in the composition of produced gas following the eighth reduction, as has been explained earlier. Further, for both those experiments, spent F6CaZ1100 was found to have only about half the density compared with fresh. Obviously, these particles changed physical properties dramatically during the experiment, which could raise doubt of the long-term stability of this material.

Summary and Conclusions

The experiments presented in this article show that freeze-granulated particles consisting of 60 wt % Fe_2O_3 supported on stabilized ZrO_2 could work well as oxygen carrier for CLC applications. The particles reacted decently with CH_4, and addition of a 5 wt % N6AM1400 particles resulted in improved fuel conversion.

The choice of stabilizing material for the ZrO_2 had some consequences on the particle properties. Mg and Ce both appear to have been working well, although the effect of adding Ni to particles stabilized with Ce was unclear. The particles stabilized with Ca initially worked well but was found to change dramatically over the course of the experiments, which prevents safe conclusions. Based on these experiences, Mg-ZrO_2 seems like the most appropriate support material for this kind of oxygen-carrier particles.

Particles sintered at 1100°C worked best. Increasing the sintering temperature resulted in harder and less porous particles, with comparably low reactivity and poor fluidization properties. Reducing the sintering temperature resulted in particles with high porosity and reactivity, but such particles also produced high concentrations of CO during the reduction.

In general, the reactivity and oxygen-carrier capacity of the better particles were comparable to that of other well-performing Fe_2O_3-based oxygen carriers, such as freeze-granulated particles of 60 wt % Fe_2O_3 supported on MgO-Al_2O_3 examined by Johansson et al.[32] It seems reasonable to believe that it will be factors such as manufacturing cost and

long-term integrity that will determine which particle composition that would be more favorable. These factors have not been addressed in this study though.

Acknowledgments

The authors thank their financers, supporters, and coworkers within the CACHET project, contract 019972 under the 6th framework program funded by the European Commission.

Notation

Abbreviations

CLC = chemical-looping combustion
C_nH_m = generic hydrocarbon fuel
F = volumetric flow (L_n/min)
F6x = generic oxygen carrier with 60 wt % Fe_2O_3 as active phase
H_{lhw} = lower heating value (J/mol)
L_n = normal liters
m = mass (g)
Me = generic oxygen carrier, reduced
MeO = generic oxygen carrier, oxidized
n = number of moles
P = pressure (Pa)
p = partial pressure (Pa)
R_0 = oxygen ratio, that is, active oxygen content of oxygen carrier (wt %)
t = time (s, min)
v = volume (L_n)
vol % = percentage by volume
wt % = percentage by weight
γ_{eff} = combustion efficiency (%)
γ_{red} = CO_2 yield (%)
ζ_{CO} = fraction of CO compared with fraction of CH_4 yield (%)
ω = mass-based degree of reduction (%)
χ = reduction in unconverted fuel by addition of NiO (%)
σ = provable synergy effect by addition of NiO (%)

Indexes

i = generic index
imp = improvement
oc = oxygen carrier
ox = completely oxidized oxygen carrier
red = completely reduced oxygen carrier
s = sample of oxygen-carrier particles
tot = total

Literature Cited

1. Cho P. *Development and Characterization of Oxygen-Carrier Materials for Chemical-Looping Combustion*. Göteborg, Sweden: Chalmers University of Technology, 2005.
2. Johansson M. *Screening of Oxygen-Carrier Particles Based on Iron-, Manganese-, Copper- and Nickel Oxides for Use in Chemical-Looping Technologies*. Göteborg, Sweden: Chalmers University of Technology, 2007.
3. Adánez J, de Diego LF, García-Labiano F, Gayán P, Abad A. Selection of oxygen carriers for chemical-looping combustion. *Energy Fuels*. 2003;18:371–377.
4. Jerndal E, Mattisson T, Lyngfelt A. Thermal analysis of chemical-looping combustion. *Chem Eng Res Des*. 2006;84:795–806.
5. Lyngfelt A, Kronberger B, Adánez J, Morin JX, Hurst P. The GRACE project. Development of oxygen carrier particles for chemical-looping combustion. Design and operation of a 10 kW chemical-looping combustor. Proceedings of the 7th International Conference on Greenhouse Gas Control Technologies, Vancouver, Canada, 2004.
6. Ryu HJ, Jin GT, Yi CK. Demonstration of inherent CO_2 separation and no NO_X emission in a 50 kW chemical-looping combustor—continuous reduction and oxidation experiment. Poster Presented at the 7th International Conference on Greenhouse Gas Control Technologies, Vancouver, Canada, 2004.
7. Johansson E, Mattisson T, Lyngfelt A, Thunman H. Combustion of syngas and natural gas in a 300 W chemical-looping combustor. *Chem Eng Res Des*. 2006;84:819–827.
8. Johansson E, Mattisson T, Lyngfelt A, Thunman H. A 300 W laboratory reactor system for chemical-looping combustion with particle circulation. *Fuel*. 2006;85:1428–1438.
9. Abad A, Mattisson T, Lyngfelt A, Rydén M. Chemical-looping combustion in a 300 W continuously operating reactor system using a anganese-based oxygen carrier. *Fuel*. 2006;85:1174–1185.
10. Abad A, Mattisson T, Lyngfelt A, Johansson M. The use of iron oxide as oxygen carrier in a chemical-looping reactor. *Fuel*. 2007; 86:1021–1035.
11. Adánez J, Gayán P, Celaya J, de Diego L, García-Labiano F, Abad A. Chemical looping combustion in a 10-kW prototype using a CuO/Al_2O_3 oxygen carrier: effect of operating conditions on methane combustion. *Ind Eng Chem Res*. 2006;45:6075–6080.
12. Linderholm C, Abad A, Mattisson T, Lyngfelt A. 160 hours of chemical-looping combustion in a 10 kW reactor system with a NiO-based oxygen carrier. *Int J Greenhouse Gas Control*. 2008; 2:520–530.
13. Linderholm C, Mattisson T, Lyngfelt A. Long-term integrity testing of spray-dried particles in a 10-kW chemical-looping combustor using natural gas as fuel. *Fuel*. 2009;88:2083–2096.
14. de Diego L, García-Labiano F, Gayán P, Adánez J, Celaya J, Palacios JM. Operation of a 10-kW chemical-looping combustor during 200 h with a $CuO-Al_2O_3$ oxygen carrier. *Fuel*. 2007;86:1036–1045.
15. Berguerand N, Lyngfelt A. Design and operation of a 10 kWth chemical-looping combustor for solid fuels—testing with South African coal. *Fuel*. 2008;87:2713–2726.
16. Berguerand N, Lyngfelt A. The use of petroleum coke as fuel in a 10 kWth chemical-looping combustor. *Int J Greenhouse Gas Control*. 2008;2:169–179.
17. Rydén M, Lyngfelt A, Mattisson T. Chemical-looping combustion and chemical-looping reforming in a circulating fluidized-bed reactor using Ni-based oxygen carriers. *Energy Fuels*. 2008;24:2585–2597.
18. Kolbitsch P, Pröll T, Bohlar-Nordenkampf J, Hofbauer H. Operating experience with chemical looping combustion in a 120 kW dual circulating fluidized bed (DCFB) unit. Proceedings of the 9th International Conference on Greenhouse Gas Control Technologies, Washington, USA, 2008.
19. Pröll A, Mayer M, Bohlar-Nordenkampf J, Kolbitsch P, Mattission T, Lyngfelt A, Hofbauer H. Natural minerals as oxygen carriers for chemical-looping combustion in a dual circulating fluidized bed system. Proceedings of the 9th International Conference on Greenhouse Gas Control Technologies, Washington, USA, 2008.
20. Brandvoll Ø. *Chemical Looping Combustion: Fuel Conversion with Inherent CO_2 Capture*. Doctoral thesis, Trondheim, Norway: Norwegian University of Science and Technology, 2005.
21. Johansson E. *Fluidized-Bed Reactor Systems for Chemical-Looping Combustion with Inherent CO_2 Capture*. Doctoral thesis, Göteborg, Sweden: Chalmers University of Technology, 2005.
22. Wolf J. *CO_2 Mitigation in Advanced Power Cycles*. Doctoral thesis, Stockholm, Sweden: The Royal Institute of Technology, 2004.
23. Kronberger B. *Modelling Analysis of Fluidised Bed Reactor Systems for Chemical-Looping Combustion*. Doctoral thesis, Vienna, Austria: Vienna University of Technology, 2005.
24. Naqvi R. *Analysis of Gas-Fired Power Cycles with Chemical Looping Combustion for CO_2 Capture*. Doctoral thesis, Trondheim, Norway: Norwegian University of Science and Technology, 2006.
25. Leion H. *Capture of CO_2 from Solid Fuels Using Chemical-Looping Combustion and Chemical-Looping Oxygen Uncoupling*. Doctoral thesis, Göteborg, Sweden: Chalmers University of Technology, 2008.
26. Rydén M. *Hydrogen Production from Fossil Fuels with Carbon Dioxide Capture, Using Chemical-Looping Technologies*. Doctoral thesis, Göteborg, Sweden: Chalmers University of Technology, 2008.
27. Jin H, Okamoto T, Ishida M. Development of a novel chemical-looping combustion: synthesis of a solid looping material of NiO/$NiAl_2O_4$. *Energy Fuels*. 1998;12:1272–1277.

28. Son SR, Kim SD. Chemical-looping combustion with NiO and Fe_2O_3 in a thermobalance and circulating fluidized bed reactor with double loops. *Ind Eng Chem Res*. 2006;45:2689–2696.
29. Adanez J, Garcia-Labiano F, de Diego LF, Gayan P, Celaya J, Abad A. Nickel-copper oxygen carriers to reach zero CO and H_2 emissions in chemical-looping combustion. *Ind Eng Chem Res*. 2006;45:2617–2625.
30. Mattisson T, Johansson M, Jerndal E, Lyngfelt A. The reaction of NiO/NiAl2O4 particles with alternating methane and oxygen. *Can J Chem Eng*. 2008;86:756–767.
31. Mattisson T, Johansson M, Lyngfelt A. CO_2 capture from coal combustion using chemical-looping combustion—reactivity investigation of Fe, Ni, and Mn based oxygen carriers using syngas. Proceedings of the Clearwater Coal Conference, Clearwater, USA, 2006.
32. Johansson M, Mattisson T, Lyngfelt A. Investigation of Fe_2O_3 on $MgAl_2O_4$ support for chemical-looping combustion. *Ind Eng Chem Res*. 2004;43:6978–6987.
33. Johansson M, Mattisson T, Lyngfelt A. Creating a synergy effect by using mixed oxides of iron- and nickel oxides in the combustion of methane in a chemical-looping combustion reactor. *Energy Fuels*. 2006;20:2399–2407.

Manuscript received Aug. 21, 2009, and revision received Nov. 10, 2009.